Femtosecond Photodissociation Dynamics of Bis(julolidine) Disulfide in Polar and Apolar Solvents

A. Lochschmidt, N. Eilers-König, N. Heineking, and N. P. Ernsting*

Institut für physikalische und theoretische Chemie der Humboldt-Universität, Bunsenstrasse 1, D-10117 Berlin, Germany

Received: July 2, 1998; In Final Form: December 2, 1998

Following femtosecond photodissociation of bis(julolidine) disulfide, the nascent geminate julolidylthiyl radicals are observed with pump/supercontinuum probe spectroscopy. The radicals are formed in a direct process within 130 fs and in a slower process over 1 ps. Two forms of the radical are distinguished by the appearance kinetics and by their spectra in polar solvents. Semiempirical calculations predict a radical doublet state D_1, optically dark and with a dipole moment of 2.3 D, close to the bright and more polar ground state D_0. The slower dissociation channel is taken to include internal conversion and relaxation within a reactive manifold of excited parent states and possibly between the accessible radical states. Subpicosecond geminate recombination is observed in viscous solvents. A dimer of the radicals is formed on longer time scales; it reacts with free radicals in a second-order reaction.

I. Introduction

The diffusion of reactive species in a homogeneous solution may be rate-determining if the reaction itself is very fast. When instead the reactants are placed close to each other initially, for example by photodissociation of a suitable precursor molecule, it becomes possible to observe the elementary reaction directly on its own time scale. In practice the photodissociation and subsequent geminate reaction are coupled, their dynamics depending on electronic states, solvent response, and spatial separation of the fragments. The photodissociation of the diatomics I_2 and Br_2 has been examined most thoroughly in this respect.[1,2] Photodissociation of iodine in compressed supercritical rare gases revealed four elementary steps: vibrational coherence during the initial phase of dissociation, solvent-induced predissociation, geminate recombination into excited electronic states, and subsequent vibrational relaxation.[3]

Much less is known about the photodissociation of larger organic molecules into neutral radicals and their geminate recombination in solution. Recall that the latter denotes the recombination of two radicals that originated from the same parent molecule. Its initial phase, when the nascent radicals recombine within the original solvent cage, is termed "primary" geminate recombination. The radicals may also first separate and then recombine after diffusive motion in the solvent. This phase is termed "secondary" geminate recombination. For large organic molecules the overall process is complicated by the high dimensionality of the potential energy surfaces for the participating electronic states (although their number should be small compared to that of iodine). Earlier work therefore seems to be restricted to only a few aromatic molecules: tetraphenylhydrazine,[4−8,10] diphenyl disulfide[9,10] and bis(*p*-aminophenyl) disulfide.[10−14] Another complication is presented by an expected orientational dependence of the cross section for recombination.[15,16] Yet apart from a desire to observe and model the dynamics of dissociation and recombination per se, we are interested in these systems because of their potential use as links in supramolecular structures. For this reason we emphasize here the femtosecond spectroscopy of organic radicals as they are generated from the excited precursor.

Tetraphenylhydrazine has been investigated with picosecond,[6,10] subpicosecond,[4,5] and femtosecond[7,8] time resolution. Following Wiersma and co-workers,[7] the photodissociation into diphenylamino radicals occurs via two different channels: one with a time constant of 80 fs, and the other within 20 ps in aliphatic solvents as deduced from time-resolved fluorescence measurements. These authors also observed a 20 ps decay of the transient absorption, which they attributed to geminate recombination. Reinvestigations by Schwarzer and co-workers,[8] who measured time-resolved transient absorption and fluorescence at various pressures in alkane solvents, showed that the decaying absorption is due to excited states of tetraphenylhydrazine, as was originally proposed by Hyde et al.[4,5] and Hirata et al.[6,10] and not to geminate recombination.

For diphenyl disulfide, Scott and Liu[9] found geminate recombination in apolar solvents on a time scale of a few tens of picoseconds by monitoring the phenylthiyl radicals at a single wavelength. They described the recombination by a diffusive model for a reactive pair in solution, as proposed by Shin and Kapral.[17] Hirata[10] used broad-band transient absorption to characterize the spectra of the nascent radicals in cyclohexane. Directly after photodissociation, a broad absorption band was observed, which evolved on a picosecond time scale into two bands at 440 and 495 nm. To assign the short time spectra, they took two candidates into consideration: an electronically excited state of diphenyl disulfide and a conformationally unrelaxed photoproduct, a phenylthiyl radical pair.

Bis(*p*-aminophenyl) disulfide (b-PAP-DS) dissociates after UV excitation into two (*p*-aminophenyl)thiyl (PAP-T) radicals. Substitution of the phenylthiyl radical by a *p*-amino group enhances the oscillator strength for the radical absorption band in the visible range and confers charge-transfer character to the lower excited electronic state. This is why the radical absorption and fluorescence bands depend on solvent polarity.[18] Hirata et al. studied the spectral evolution and dimer formation in

* To whom correspondence should be addressed.

10.1021/jp982846j CCC: $18.00
Published on Web 03/05/1999

n-hexane on a picosecond time scale.[10,12,13] They observed an instantaneous absorption band centered at 560 nm, which narrowed exponentially, and a delayed broad absorption band at 650 nm, which decayed in hundreds of picoseconds. The former band was ascribed to (*p*-aminophenyl)thiyl radicals and the latter to the formation of radical sandwich dimers. The absorption due to sandwich dimers decreased significantly with increasing solvent polarity. These results were compared with molecular orbital calculations, and activation energies were estimated for geminate recombination and dimer formation. Using femtosecond broad-band absorption spectroscopy, Bultmann and Ernsting[14] reported a competition between geminate recombination and solvation of the photolytically generated radicals in polar solvents. The photodissociation occurred in the range of 40−100 fs. The subsequent time-dependent red-shift of the radical bands was assigned to solvation dynamics. Primary geminate recombination was observed in viscous solvents, and the caging behavior in the first 2 ps was explained by a macroscopic diffusion model.[19] For times after 2 ps, it was concluded that solvation stabilizes the radicals and thus creates an activation barrier for further recombination. In polar solvents of low viscosity no recombination was observed.

The present paper continues the study of the photodissociation of aromatic disulfides. Our aim is to get more insight into the spectroscopy of the thiyl radicals and into their primary and secondary geminate recombination. Following earlier results[14] summarized above, we expect a higher recombination yield in aliphatic solvents where the radicals should be only weakly stabilized by polar solvation. Because of better solubility in apolar solvents and hence wider use in radical solvation studies, we examine bis(julolidine) disulfide (b-JUL-DS) and its photodissociation products, the corresponding 9-julolidylthiyl (JUL-T) radicals:

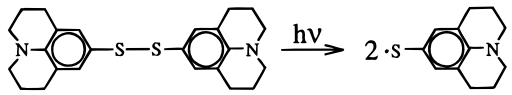

Ishizaka[20] was the first to investigate their fluorescence and lasing properties. Here we report mainly the transient broad-band spectroscopy of the nascent radicals in polar and apolar solvents on femto- and picosecond time scales. Assignments are guided by semiempirical quantum-chemical calculations and are further supported by results from absorption measurements with microsecond time resolution.

II. Experimental Section

Femtosecond pulses at 630 nm with 90 fs intensity autocorrelation (AC) width (fwhm) are generated with a colliding-pulse-mode dye laser (pumped with 1 W at 514 nm of a Lexel 3500 Ar^+ laser). In a three-stage dye amplification driven by the second harmonic of a seeded Nd:YAG laser (Continuum PL6030) at 30 Hz, the pulses are amplified to 160 μJ with 1% of energy background from amplified spontaneous emission. The amplified short pulses are recompressed to an AC width of 85 fs. The energy after recompression is 140 μJ/pulse in a diffraction-limited beam.

For the pump-and-probe spectroscopy, the basic beam is split in two parts. One part (30%) is used to generate the UV pump pulses. It is focused with a 1300 mm lens onto a 150 μm KDP crystal for frequency doubling. The output energy is about 8 μJ for 45 μJ input. The second part, after passing a variable delay stage, is used to generate supercontinuum probe pulses. It is focused with a 400 mm lens into a water flow cell (thickness 2 mm, 170 μm glass windows). The continuum is first passed through a thin spectral filter made from dye solutions and then routed by dispersion-free, anastigmatic optics[14] through the sample cell. At the sample the optical axes for pump and probe beam cross at an angle of 18°. The continuum beam diameter in the sample is less than 200 μm, and the UV pump beam diameter is 500 μm; a typical pump pulse energy is 6 μJ. The probe polarization is set to the magic angle with respect to the pump polarization. Before passing the sample the continuum beam is split into reference and probe beams. Sample and reference data are dispersed by home-built Rowland-type polychromators[21] and recorded with photodiode arrays (Hamamatsu). These data are used to determine the change of optical density, ΔOD, as a function of wavelength for every shot. Typically, 50−75 spectra are averaged for the final transient spectrum at a given delay position. To record the baseline, every second pump pulse is blocked.

To determine the time resolution, the cross-correlation (CC) between the pump pulse and spectral components of the continuum was derived from the rise of the excited-state absorption of 1-methylnaphthalene. Excitation at 315 nm in a 1 mm quartz cell gave a CC time (fwhm) of 105 fs, assuming Gaussian pulses. The time-zero delay position was obtained from the response peak of the neat solvent[22] for different wavelengths over the entire spectral range from 360 to 800 nm. Spectra were recorded for three time series: 0−5 ps with step sizes of 7 and 14 fs, 0−50 ps with 0.2 ps, and 0−250 ps with 2 or 4 ps step size. The spectra of the first series were corrected for the measured dispersion of time-zero.

The contamination of cell windows by photoproducts is a serious experimental problem in disulfide dissociation studies, especially with unpolar solvents. This is why CaF_2 windows (1 mm) were used, since they have low affinity for surface adhesion. For an acceptable signal-to-noise ratio at disulfide concentrations below 10^{-3} M, the usual 300 μm internal path length of the sample cell was increased to 1 mm. The CC time in this case was $\leq$200 fs. To minimize a broad background observed for the highly viscous alkanes, the pump pulses were attenuated to 2 μJ by neutral density filters.

Microsecond flash photolysis experiments were performed with a detector setup similar to the femtosecond experiments. Excitation at 308 nm was provided by a XeCl* laser. White probe light from a xenon lamp (0.7 μs pulse width) was split into reference and probe beams, passed through a 10 mm quartz probe cell and was detected by Rowland-type polychromators equipped with photodiode arrays. The trigger of the xenon lamp was delayed with respect to the trigger of the excimer pulse. The probe volume of ca. 10 × 1 × 1 mm was overlapped completely by the pump beam. Given this probe volume and pump overlap, an influence of diffusion on the observed microsecond kinetics can be ruled out.

For the EPR experiments, b-JUL-DS was dissolved (10^{-4} M) in a 1:1 mixture of *n*-pentane and 2-methylbutane. A glassy sample was formed by immersion into liquid N_2. Only after subsequent irradiation with a mercury−xenon lamp were EPR signals detected; the microwave frequency was 9.28 GHz, and the reference standard was Cr^{III}.

b-JUL-DS was synthesized as described in ref 23. All solvents were of spectroscopic grade. Concentrations were 0.2−0.5 mM for femtosecond measurements and 0.02−0.05 mM for microsecond measurements.

III. Results

A. Observation of EPR. The **g** tensor of the observed species is anisotropic, with values $g_\perp = 2.006 \pm 0.001$ and $g_\parallel = 2.032$

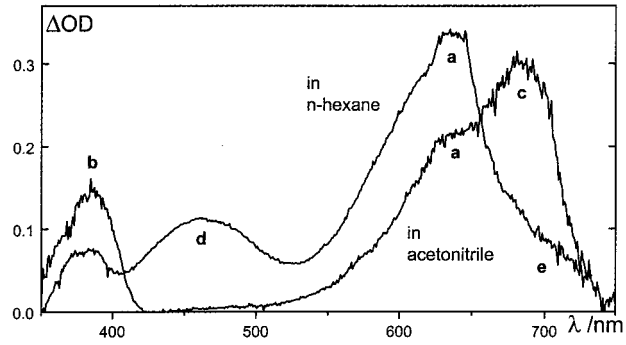

Figure 1. Absorption spectra in *n*-hexane and acetonitrile, 10 μs after photolysis of bis(julolidine) disulfide at 308 nm. (Labels a−e are used in the text to identify spectral features.)

$\pm$ 0.001. This is in reasonable agreement with $g_\perp = 2.0078$ reported for the *p*-(aminophenyl)thiyl radical.[24] As no paramagnetic behavior was observed prior to UV irradiation, we assign the observed signal to photolytically produced julolidylthiyl radicals. The stability of substituted phenylthiyl radicals at low temperatures has been reported earlier.[25,26] The irradiated samples were of a turquoise color, which faded upon heating to ambient temperature.

B. Transient Absorption with Microsecond Resolution. The absorption spectra after photolysis of b-JUL-DS at microsecond delay times are different for polar and apolar solvents. Figure 1 summarizes and compares the main observations for two solvents, acetonitrile and *n*-hexane. Common features in both cases are a strong band in the red around 630−640 nm (labeled a in the figure) and a weaker band in the near UV at 385 nm (b). In polar solvents there appears an additional, even stronger band at 670−690 nm (c). The peak positions of the red bands (a and c) depend on solvent polarity. A broad band in the blue around 465 nm (d) and a spectral wing in the deep red near 690 nm (e) are observed only in apolar solvents. The latter is kinetically distinct from band c (see below). All of these components are observed up to hundreds of microseconds, and none appears to be sensitive to dissolved oxygen.

Next we consider the spectral evolution on the microsecond time scale. In polar solvents, all bands (one UV and two red bands) exhibit approximately the same relative intensity decrease. This drop is considerably steeper in methanol compared to propylene carbonate. In apolar solvents, the relative decrease is different for the three discernible bands (UV slowest, blue steepest, and red between). The shoulder at 690 nm behaves similarly to the blue band. Analyses of the first and central second spectral moments of the red band in apolar solvents reveal a minor blue shift of a few nanometers and a distinct narrowing by about 10 nm, both on a 100 μs time scale, which is correlated with the disappearance of the blue band. Shift and narrowing are absent for the blue band.

C. Transient Absorption with Subpicosecond Resolution. Transient spectra on a picosecond time scale after photodissociation are shown in Figure 2. The spectra have been corrected for the dispersion of time zero. The upper panel gives transient absorption spectra in 2-methylbutane as representative for all apolar solvents studied. As in the microsecond spectra, three contributions are clearly recognized: the UV band, the broad blue band around 460 nm, and the main band at 630 nm with a wing in the deep red. The lower panel shows transient spectra in acetonitrile representing the polar solvents. As in apolar solvents, they show the absorption band around 630 nm and the weaker band in the near UV. In comparison with the spectra

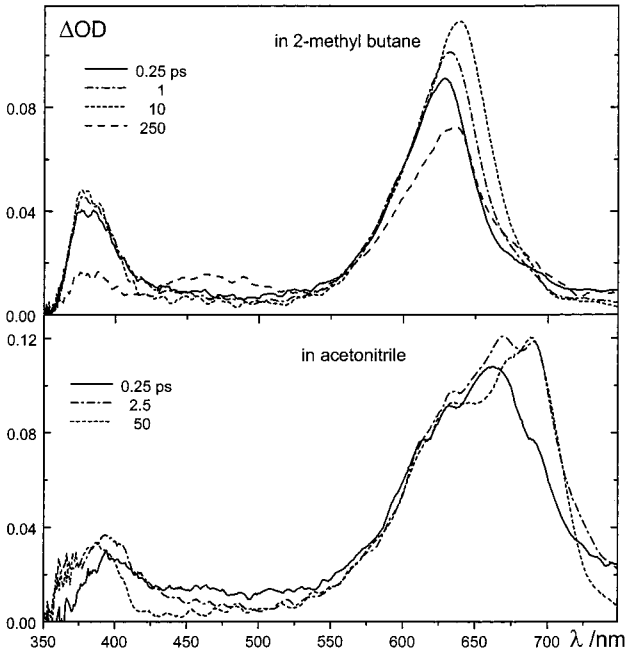

Figure 2. Transient absorption spectra in 2-methylbutane and in acetonitrile for delay times, after photolysis, in the femtosecond and picosecond range.

in apolar solvents, the main band is broadened by a contribution at 690 nm. The UV band is also located further to the red.

Spectral evolution is observed on various time scales.

Instantaneous: Within the CC time a very broad and structureless absorption rises over the entire spectral range.

Up to 1 ps: The absorbance in the UV band and in the red band appears with a deconvoluted rise time of 100−150 fs, but the full amplitude is not reached by this step. At the low energy side of both bands a wing is observed, which is more intense in highly viscous solvents.

Up to 5 ps: The broad, structureless absorption disappears within the first picoseconds. Also the absorption in the wings on the red side of the bands decreases over a few picosecond depending on solvent viscosity. The red band of lower energy and the UV band experience further rise during the time interval up to 10 ps. In apolar solvents, where only one red band is observed, its amplitude rises with a fast (100−150 fs) and a slower (ca. 1 ps) component. In highly viscous solvents the entire red band (in polar solvents predominantly the component at higher energy) decreases over 3 ps. This effect is most clearly seen in Figure 3 for propylene carbonate as solvent.

Up to 200 ps: In some tens of picoseconds both bands (UV and red) decrease in less viscous alkanes, while a new broad blue band at 460 nm appears. Additionally, a wing in the deep red at 690 nm evolves on virtually the same time scale as the blue band. In highly viscous alkanes the evolution is similar but less obvious. In polar solvents, on the other hand, there is virtually no evolution on this time scale.

D. Data Analysis. The transient absorption spectra clearly consist of several contributions. They will later be associated with absorption by the radicals (one UV and two overlapping red bands), excited-state absorption by the parent disulfide (broad structureless background at time zero), its bleaching at the higher energy side of the UV band, and—in apolar solvents only—dimer formation within 100 ps (broad blue and deep-red bands). Regardless of assignments, though, the spectra are described most naturally by overlapping contributions with varying amplitudes in the course of evolution. Rather than

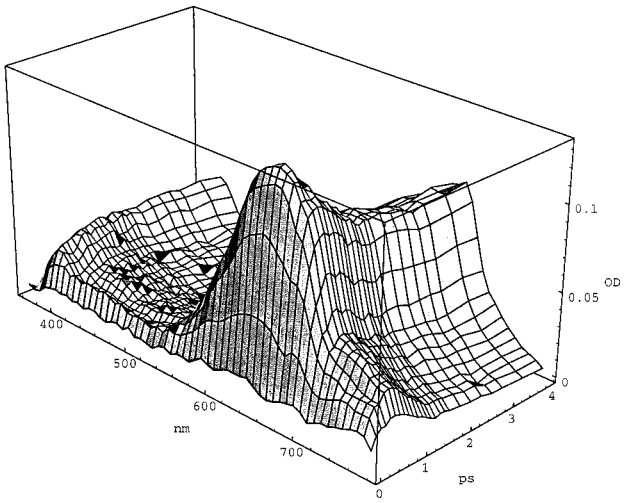

Figure 3. Spectral evolution of the transient absorption spectra in propylene carbonate during the first 4 ps.

interpreting the change of absorbance at various wavelengths, one may alternatively discuss the evolution of just a few amplitudes or similar measures. It is with this empirical approach in mind that we decompose the transient spectra into component bands. In apolar solvents at 10 ps, e.g., the red absorption band around 630 nm may be taken as a first basic spectral component. Its shape is described empirically by a blue-degraded progression of three Gaussian distributions over wavenumbers, with common width (925 cm^{-1} fwhm), equal spectral separations (1100 cm^{-1}), and fixed amplitude ratios (0.08:0.4:1). The dominant Gaussian of this progression is centered at 15 730 cm^{-1} in 2-methylbutane. All other components are described by single Gaussians. For apolar solvents in the subpicosecond series, it was not necessary to account for the deep-red wing at 690 nm. In the picosecond series it had to be fixed in position and width to avoid unphysical results. For polar solvents, the red absorbance structure was covered by the progression mentioned above (with its dominant band centered at 15 540 cm^{-1} in acetonitrile, for example) and by an additional component around 14 600 cm^{-1} representing the low-energy contribution, with variable position and width. The broad blue band and the UV-band were likewise described by single Gaussians. The higher energy side of the latter ($\geq$27 400 cm^{-1}) was excepted from fitting since bleaching of the parent disulfide overlaps with the UV band in this spectral region, especially in polar solvents. For early times the position for the UV component was fixed to that at 5 ps. The broad background absorption was described by a linear baseline over the entire frequency range, based on the region between the UV and main bands for polar solvents and additionally on the 750−780 nm region for apolar solvents.

All fits started at maximal delay where good convergence was reached. The fitting procedure then ran in reverse direction to the region of time zero where convergence deteriorated due to strongly overlapping bands. Start parameters for the main band and the UV band were optimized at 10 ps delay, while the rest was determined at 200 ps. Figure 4 shows the decomposition of transient spectra at 50 ps, for 2-methylbutane (Figure 4a) and acetonitrile (Figure 4b). With such decomposition for every time step it is possible to trace the evolution of the peak absorbance of a band, of its mean frequency, or of the integrated absorbance for spectral regions. The corresponding traces are presented in Figures 5−8; they represent the main experimental results of this work. Also shown in Figures 5 and 6 are fits to these traces, of a convolution of the Gaussian apparatus function and (at the most) the sum of two exponential

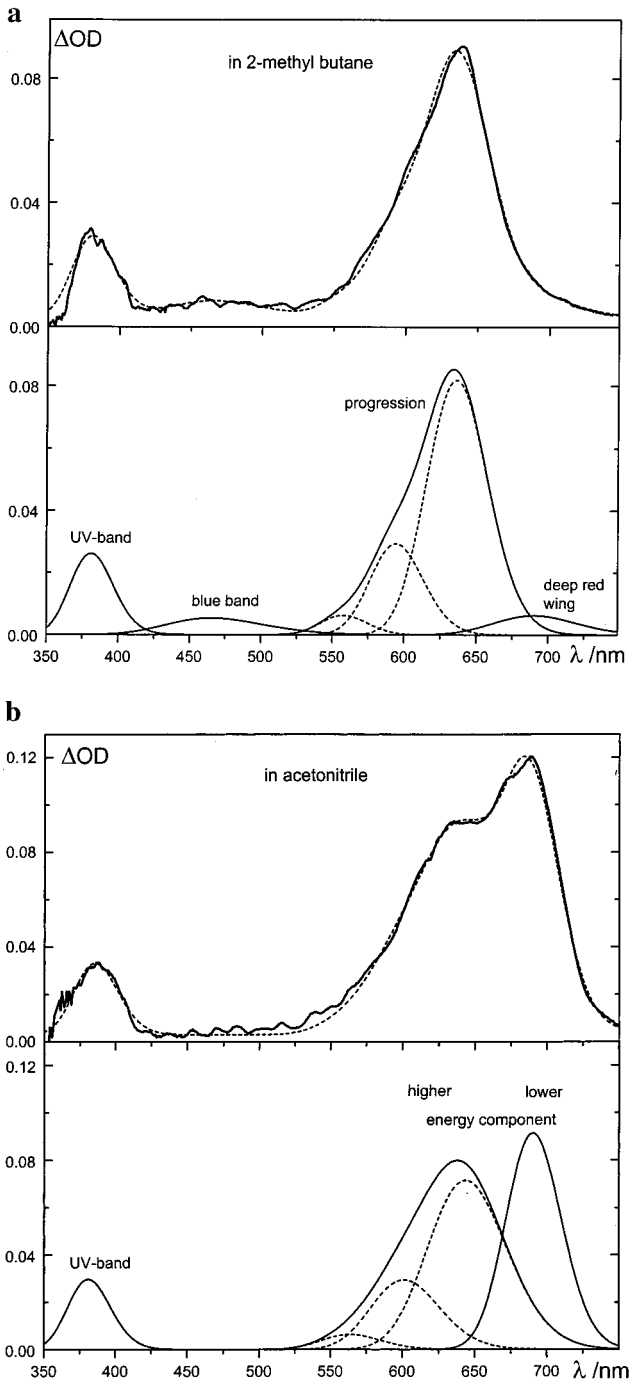

Figure 4. (a) Transient absorption spectrum in 2-methylbutane at 50 ps (upper panel, solid line) and its empirical description by a sum of Gaussian functions (dashed line). The Gaussian components are shown in the lower panel. (b) Transient absorption spectrum in acetonitrile at 50 ps (upper panel, solid line) and its empirical description by a sum of Gaussian functions (dashed line). The Gaussian components are shown in the lower panel.

terms. The relative error of the picosecond time constants thus obtained, and given below, is approximately ±10%, as judged from fits to data from different experiments.

Figure 5 shows the evolution in aliphatic solvents at early time up to 3 ps, of the peak absorbance of the red band and the UV band. In 2-methylbutane (upper panel), both bands rise in two phases: a fast rise with an estimated time constant $\tau_1 \approx$ 130 fs and a delayed rise with $\tau_2 \approx 1$ ps. In *n*-hexadecane (lower panel), the fast rise of the red band is followed by a partial decay with a 0.6 ps time constant. Since the UV band has a

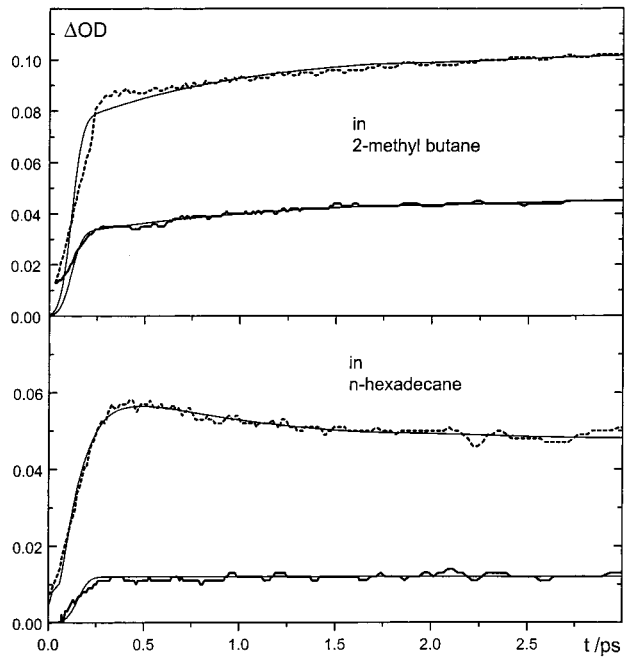

Figure 5. Evolution of the peak absorbance for the red band (dashed line) and for the UV band (solid line) in 2-methylbutane and in *n*-hexadecane and corresponding biexponential fits (thin solid lines).

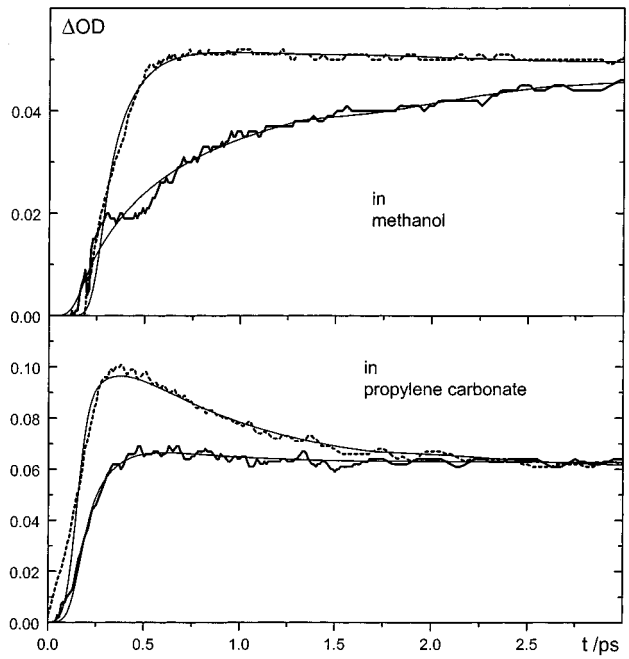

Figure 6. Evolution of the high- and low-energy components of the red band (dashed and solid lines, respectively) in methanol and in propylene carbonate. Shown are the peak absorbance for the two spectral components and corresponding biexponential fits.

smaller amplitude, it is more susceptible to systematic errors in assessing the background contribution. This may be the reason the decay of the red band is not directly mirrored by the UV band. From a qualitative perspective, however, note that the delayed rise of the UV band in nonviscous 2-methylbutane has been reduced to constant absorbance for viscous *n*-hexadecane, in accordance with the reduction for the main band absorbance when the solvent viscosity is increased.

The spectral evolution in methanol and propylene carbonate is compared in Figure 6. As was mentioned earlier, in polar solvents the red part of the spectrum is broader and more

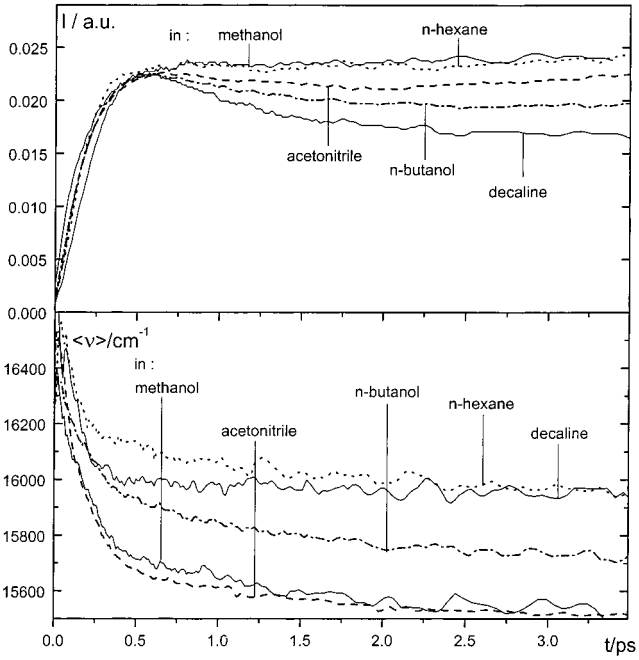

Figure 7. Evolution of the integrated absorbance $I = \int \Delta\mathrm{OD}\, d\nu$ (upper panel) for the red spectral bands and of the corresponding first spectral moment (lower panel) in several solvents.

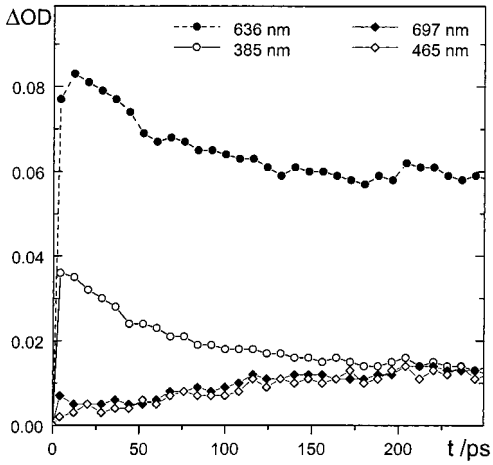

Figure 8. Evolution of the radical absorption bands (amplitudes) in 2-methylbutane, over a larger picosecond delay range.

structured compared to solutions in 2-methylbutane. The figure gives the evolution of the two spectral components in that region, represented by a progression as described above and by a Gaussian centered at ≈690 nm, respectively. In methanol (upper panel) the peak absorbance of the higher energy component remains constant after a fast rise. The component at lower energy, after a small initial rise, continues to rise on a picosecond time scale. Again, a change of solvent from methanol to the more viscous propylene carbonate (lower panel) modifies both curves in the same manner: the early parts are relatively unaffected while the ΔOD values after 0.5 ps are reduced compared to the methanol solution.

Figure 7 summarizes the evolution of the integrated absorbance $I = \int \Delta\mathrm{OD}\, d\nu$ for the red region and of the mean frequency there, for a number of solvents up to 3 ps. For example, the slight delayed rise of integrated absorbance of the red region for methanol (upper panel) is due to the delayed rise of the low-energy contribution to the composite spectrum (cf. Figure 6). The influence of that contribution, which is allowed to shift in time, is more pronounced on the mean transition

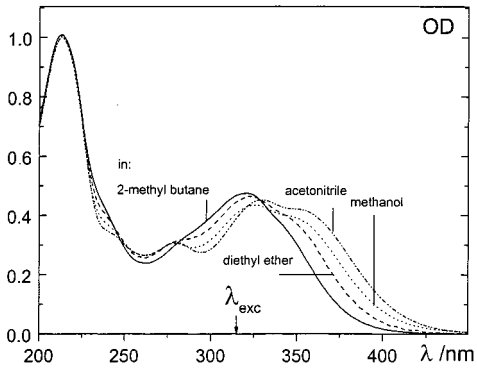

Figure 9. Stationary absorption spectra of the parent bis(julolidine) disulfide in various solvents.

frequency (lower panel), which shifts to the red by several 100 cm^{-1} in two phases. The amplitude of the shift is larger for the polar solvents in the first phase before 0.5 ps, after which time the further shifts are similar for apolar and polar solvents.

The last Figure 8 in this section shows the spectral components on a much longer time scale for 2-methylbutane as solvent. The main bands, red and UV, decay initially with a 55 ± 6 ps time constant, while the broad blue band and the deep red wing rise with an 80 ± 8 ps time constant.

IV. Discussion

A. Semiempirical Calculations. To better understand the evolution of the spectra, semiempirical calculations on a multiconfiguration SCF level were performed. We used the SAM1/d Hamiltonian (Semichem's AMPAC 5.0), which accounts explicitly for the sulfur d orbitals. Typically, 100 selected permutations (in some cases 316) from a basis of the four highest occupied (HOMO) and four lowest unoccupied (LUMO) orbitals, or sometimes from the three HOMOs and three LUMOs, were involved in the configuration interaction (CI) calculations. Increasing the number of CI orbitals changed the results only marginally and therefore does not affect the qualitative discussion below. For the excited singlet states of b-JUL-DS, two electrons were explicitly divided between two orbitals (keyword OPEN(2,2)). Most of the calculations were performed for both the parent b-PAP-DS (or the radicals PAP-T) and b-JUL-DS (or JUL-T). However, with the exception of structural details at the nitrogen atoms, there were no major differences. For the ground states of the disulfides we found structures very close to C_2 symmetry, with CSSC dihedral angles slightly larger than 90° and SS bond lengths around 213 pm. The amino groups were virtually coplanar with the phenyl rings in the case of b-PAP-DS but slightly tilted or bent out of plane in the case of b-JUL-DS. The geometry for the first excited state could not be optimized unless the SS bond length was kept fixed; for successively increased values for this bond length, the resultant energy decreased. We take this as an indication of the dissociative character of this state. Our calculations suggest the existence of at least three further excited states in relative proximity to the first excited state. The configurational expansion coefficients and energetic ordering of these states depend strongly on structural details such as torsional angles; therefore, we refrained from a more detailed analysis of their structures. It should be mentioned, however, that in our experiments the initial excitation occurs into one of these states, as may be inferred from the absorption spectrum of b-JUL-DS in Figure 9. Similar conclusions were reached by Maier et al. in a quantum-chemical study of aromatic disulfides.[27]

Interestingly, the partial geometry optimization for increasing values of the SS bond length resulted in distinctly different changes in the two thiyl moieties. While one of these developed markedly alternating CC bond lengths, the other showed a pronounced shortening of the CS and CN bond lengths. This was accompanied by an opening of the CSSC dihedral angle toward a trans-like structure. Between ca. 270 and 290 pm, no convergence could be achieved; beyond 290 pm, the calculations converged basically to two radicals in the electronic states D_0 and D_1 (see below). At this distance, similar results were obtained for the lowest triplet state of total spin, corroborating the picture of two virtually unbound radicals. The T_1 state could be optimized to a very shallow potential minimum of C_{2h} symmetry at ca. 230 pm SS bond length.

The radicals were studied in more detail. These calculations were performed without symmetry restrictions. The molecular symmetry in the radical ground state was obtained close to C_{2v}. The latter symmetry is broken only by the conformation of the ethylene bridges that brace the amino group. For labeling the orbitals, it is therefore convenient to employ a C_{2v} reference structure. Let x denote the N−C···C−S symmetry axis, y the in-plane axis, and z the axis normal to the phenyl ring. The species a_2 is symmetric with respect to rotation around x, b_1 symmetric with respect to reflection in the xy plane, and b_2 symmetric with respect to reflection in the xz plane. The molecular orbitals may then be characterized as follows: b_2 (π, HOMO-2), b_1 (n_S, HOMO-1), b_2 (π^*, HOMO), a_2 (π^*, LUMO), b_2 (π^*, LUMO+1). Thus the doublet ground state D_0 has approximately B_2 electronic symmetry. The D_1 state was found only ca. 0.5 eV above the D_0 state, with reduced dipole moment (2.3 D vs 6.4 D) and substantially different bond lengths. It results from the excitation HOMO-1 → HOMO of an electron from a pure in-plane p_y orbital at the sulfur atom (n_S) into a somewhat extended π^* orbital with a dominant coefficient for the sulfur p_z orbital. Therefore its electronic symmetry is labeled B_1. The next higher state D_2 (dipole moment ≈ 9 D) is a mixture of the excitations (HOMO-2) → HOMO and HOMO → (LUMO+1), which all have b_2 symmetry. Hence the $D_2 \leftarrow D_0$ optical transition is allowed and polarized along the symmetry axis. It can be associated with the red band observed at 630 nm for the JUL-T radical. The $D_2 \leftarrow D_1$ transition, which might be expected ca. 4000 cm^{-1} to the red if D_1 were populated by the photodissociation, is not allowed optically. The UV band at 385 nm can be assigned to the $D_3 \leftarrow D_0$ transition.

The D_0 and D_1 JUL-T radicals have small energy barriers at the C_{2v} conformations, separating local minima of C_2 (tilted) and C_s (pyramidal) symmetry from each other (and from their enantiomeric counterparts). In the D_0 state, these conformations have approximately equal energies, whereas in the D_1 state the twisted form is calculated to be more stable by about 9 kcal/mol.

It is not clear which radical species are initially formed in the dissociation of bis(julolidine) disulfide. As CS-bond cleavage is much less likely than breaking of the SS bond, let us consider the formation of two julolidylthiyl radicals only. Energetically, the D_0 and D_1, possibly even the D_2, states of the radicals are accessible in a number of combinations. All of these can, in principle, form conformers of C_2 and C_s symmetry. Furthermore, at least two triplet states are within the accessible energy range. From these calculations there is little reliable information on the accessibility and relative stability of more loosely bounded radical dimers of whichever total spin.

B. Interpretation of the Early Transient Spectra. Which of the states and conformers are seen directly after photodis-

sociation on femtosecond and picosecond time scales? To begin with, consider the similarity of the rise of the red and the UV band in nonviscous, nonpolar solvents. This observation supports the previous assumption that these bands belong to the same species. For viscous solvents, the fast rise of the red band is immediately followed by partial decay. From this we conclude that the absorbing species is able to recombine within the solvent cage. (As was already mentioned in the Results, in polar solvents the recombination process is countered by the delayed rise of the lower-energy red band). We conclude that two julolidylthiyl radicals are formed, but that—as predicted by the semiempirical calculations—transient absorption observes only those in the D_0 state. Several electronic states participate in the photodissociation process (cf. Figure 10): up to four states of the excited b-JUL-DS parent molecule, and at least two receiving states, D_0 and D_1, for each of the geminate JUL-T radicals. Therefore, the biphasic rise of the observed D_0 population, with $\tau_1 \approx 130$ fs and $\tau_2 \approx 1$ ps, may reflect a fast photodissociation channel directly feeding D_0 and a slower channel that involves intermediate dark states. The decay of a broad background underlying the early spectra is somewhat faster than the rise of radical absorbance. The background should therefore be assigned to absorption from the excited states that are passed in the slower channel.

This model was used by Wiersma and co-workers[7] to describe the photolysis of tetraphenyl hydrazine in alkane solutions. They assumed a reaction from more than one excited state of the parent molecule leading to a delayed rise in the radical population. As regards the dissociation step, Schwarzer and co-workers[8] essentially corroborated this model. These authors proposed an activationless direct process and a slower channel with a solvent-dependent barrier for the photodissociation.

For the photodissociation of bis(julolidine) disulfide, however, the situation is even more complex. The radical absorption in the red part of the spectrum becomes broad and more structured in polar solvents (cf. Figure 1). As regards the early evolution of that structure, the high-energy component (630 nm) appears fast while the low-energy component (690 nm) shows a delayed rise (cf. Figure 6). In the following we present our hypothesis for the photodissociation process. In principle, photolysis channels leading to products other than JUL-T radicals (for example C−S cleavage) are also conceivable. However, that scenario is unlikely for energetic reasons and in view of the spectro-temporal data, which show strong absorption typical of JUL-T radicals after one picosecond. Therefore, our basic assumption is that only JUL-T radicals emerge from the photolysis of b-JUL-DS on a subpicosecond time scale, as was already suggested by the semiempirical calculations of the previous section. Yet there are two distinct spectral components on the subpicosecond to picosecond time scales. These two components cannot be associated with population in the pure electronic states D_0 and D_1 of the radicals since the latter state should not absorb in this range. Within the context of our semiempirical calculations, the structure of the red band must be explained as due to two different conformers of the radical in the D_0 electronic state. The observed two radical forms have similar spectra, which, however, may be partially distinguished by varying the solvent polarity. That distinction in turn suggests that the two forms, although they derive their oscillator strength from the D_0 state, nonetheless should have a different dipole moment, which implies vibronic coupling to the D_1 state. Further work is clearly needed on these structural and electronic aspects. The direct dissociation channel is apparently more efficient and gives both forms while the delayed channel, passing through intermediate states, finally gives predominantly the more polar radicals. In apolar solvents the two spectra are no longer distinguished and are therefore superimposed, resulting in a biphasic rise.

Let us compare the rise of the JUL-T radical bands with that of the related PAP-T radical. Earlier work on radical generation in diethyl ether showed a delayed rise but no spectral structure.[11] Neither delayed rise nor spectral structure for the radical absorption of PAP-T radicals in polar solutions was reported by Bultmann et al.[14] Using an excitation energy lower by 4000 cm^{-1}, Lysak et al.[28] observed a slow rise of a red-shifted shoulder in the absorption spectrum of the same molecule in ethanol. Taken together, the experiments imply the involvement of different intermediate states depending on excitation energy relative to the disulfide absorption band, in accordance with the general model above. The former work focused on geminate recombination and solvation of the nascent PAP-T radicals. The absence of recombination in methanol and ethanol was attributed to fast solvent relaxation stabilizing the radicals. Hence geminate recombination should be enhanced in apolar solvents, for example, in *n*-hexane. In the present work we do not observe primary geminate recombination of JUL-T radicals in that solvent. We are forced to conclude that polar solvation of the JUL-T radicals is not crucial in hindering their geminate recombination.

C. Interpretation of the Microsecond Spectra and Kinetics. A collision of two free radicals R may produce the disulfide parent P or (in principle) a radical dimer D. Following the photodissociation of b-PAP-DS in *n*-hexane, Hirata *et al.*[13] observed a broad transient absorption band in the red, which they assigned to the PAP-T sandwich dimer. In this case the dimer band was formed with a rate similar to the decay rate for the free radical absorption (time constant of 60 ps); it disappeared over several hundred picoseconds with first-order kinetics. During the initial period the formation rate of the sandwich dimer should overcome its unimolecular decay, which is dominated by secondary geminate radical recombination.

Let us return to the photolysis of b-JUL-DS. By analogy we assign the broad blue band at 465 nm and the deep-red wing at 690 nm, which are only observed in apolar solvents after tens of picosecond, to a radical dimer. Thus, the UV band is associated only with the free radical and the blue band only with the dimer. This JUL-T dimer appears to be quite stable compared to the PAP-T dimer mentioned above, although decaying faster than the JUL-T radicals, as gauged by the disappearance of the blue band relative to the UV band. For an interpretation of that decay, the most probable channel is the collision with a free radical, by which the parent disulfide is formed and one of the radicals in the dimer is liberated. In this case we have the following kinetic scheme (here P stands for parent, R for radical, and D for dimer; α is the percentage of dimer-producing recombinations):

$$R + R \rightarrow P \qquad (\{1 - \alpha\}k_1)$$

$$R + R \rightarrow D \qquad (\alpha k_1)$$

$$R + D \rightarrow P + R \qquad (k_2)$$

$$D \rightarrow R + R \qquad (k_3)$$

The dominant processes are nongeminate recombination and reactive radical−dimer collisions; superimposed is an equilibrium between free radicals and dimers. Because of the diminishing overall radical concentration, the dimer concentration decreases faster than the free radical concentration. The ratio

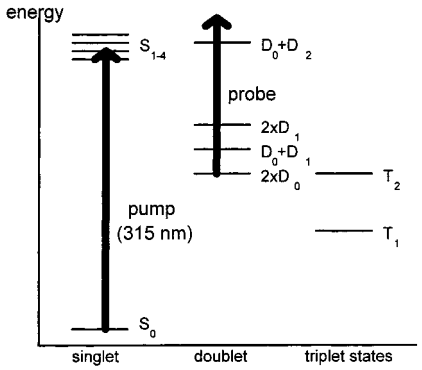

Figure 10. Schematic energy diagram for the dissociation of bis-(julolidine) disulfide into two julolidylthiyl radicals. S and T indicate the parent singlet and triplet states; D indicates the radical doublet states.

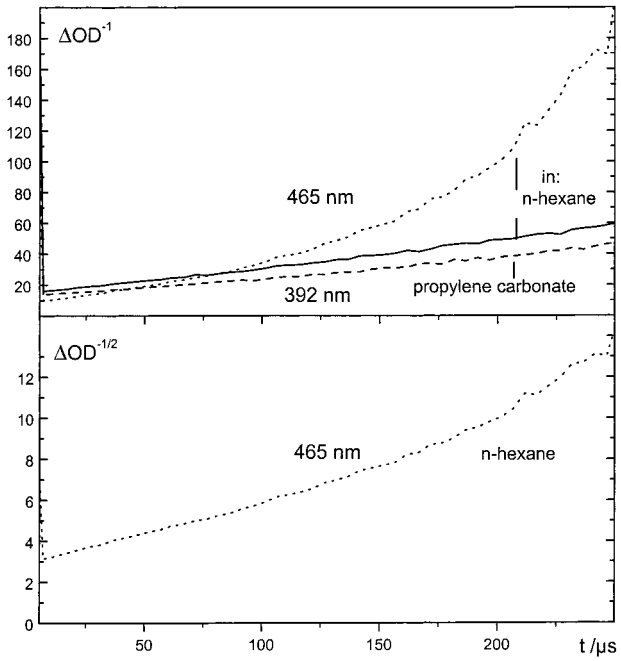

Figure 11. Plot of microsecond kinetic data for the UV and blue bands. Upper panel: ΔOD^{-1} vs time in *n*-hexane and propylene cabonate. Lower panel: $\Delta OD^{-1/2}$ vs time in *n*-hexane. The displayed time range corresponds to the decay of the signal to three-fourths of its maximum value.

of rate constants for *secondary* geminate recombinations to the disulfide and to the dimer is approximately 1:2, as estimated from the different decay and rise times of the UV and blue bands, respectively, in the picosecond experiments (cf. Figure 8). If this ratio also applies to *nongeminate* recombinations, then α should have a value around 2/3. On this time scale unimolecular dimer dissociation is probably not negligible but is obscured by the more efficient radical-dimer collision process. Nevertheless, unimolecular dissociation tends to maintain a radical/dimer equilibrium. Therefore, there exists an approximately constant concentration ratio $[D]:[R]^2 \approx \alpha k_1:k_3$. If this is inserted in the rate equations, one obtains a second-order expression for $d[R]/dt$ but $d[D]/dt \propto [D]^{3/2}$. This consequence from the kinetic scheme is tested in Figure 11. The top panel represents the reciprocal of the induced optical density and therefore aims at exposing second-order kinetics. Indeed, a plot of $(\Delta OD_{392\ nm})^{-1}$ vs time gives almost a straight line, both for *n*-hexane and propylene carbonate as solvents, in accordance with the assignment of the UV band to the recombining radical R. However a time plot of $(\Delta OD_{465\ nm})^{-1}$ for the blue band is markedly curved in this panel, which indicates that the corresponding species is not the radical. The lower panel, on the other hand, shows a plot of $(\Delta OD_{465\ nm})^{-1/2}$ vs time. If the assignment to the radical dimer D and the kinetic scheme above are correct, then an approximately straight line is expected. This is indeed observed, consistent with the scheme above. Finally, the microsecond decay of the red band (integrated absorbance) after b-JUL-DS dissociation in 2-methylbutane was observed to fall between that of the UV band and the blue band. This may be explained by the composite nature of that band, since absorption by free radicals and by the dimer overlap here.

V. Conclusion

Julolidylthiyl radicals, like the related (*p*-aminophenyl)thiyl radicals, are formed efficiently by photodissociation of the corresponding disulfide. They are characterized by an intense absorption band in the red and a weaker UV band. Using pump/supercontinuum probe spectroscopy, we observe the appearance of the radical absorption after femtosecond excitation of the parent disulfide in polar and apolar solvents and follow its change with 100 fs time resolution. In combination with semiempirical calculations for the parent disulfide and the radicals, the following picture emerges.

Dissociation involves several close-lying electronic states of the parent disulfide.

The geminate radicals may each be produced in the doublet ground state D_0 or in a low-lying dark state D_1, which is less polar than D_0, according to semiempirical calculations.

Two forms of the radical are produced. Their optical spectra are practically identical in apolar solvents, with an intense absorption maximum at 630 nm. In polar solvents, one form retains the absorption band at 630 nm while the other has an absorption maximum at 690 nm. The involvement of the electronic states D_0 and D_1 in the two forms needs to be clarified.

Photodissociation at 315 nm generates radicals via two channels. A direct channel, with a rise time of ≈130 fs, generates both forms. A delayed channel, with rise time on the order of 1 ps, leads mainly to the radical form absorbing at 690 nm in polar solvents. The delayed rise is attributed to internal conversion between the various electronic states, for both the excited parent and the geminate radicals, before an optically bright radical ground state is reached.

In viscous solvents, primary geminate recombination is observed on a subpicosecond time scale. In *n*-hexane, fast recombination is not observed. This means that for julolidylthiyl radicals, the idea that removal of polar solvation would enhance early geminate recombination is not tenable.

The geminate radicals also recombine to form a dimer that is characterized by broad absorption bands at 465 nm and at 690 nm. The dimer reacts in a second-order reaction with free radicals, to form the parent disulfide and thus liberate the other radical of the dimer.

Acknowledgment. We thank R. Stösser for conducting the EPR experiment. We also thank I. Gerhardt for synthetic work. Financial support by the Deutsche Forschungsgemeinschaft and the Fonds der Chemischen Industrie is gratefully acknowledged.

References and Notes

(1) Schroeder, J.; Troe, J. *Anu. Rev. Phys. Chem.* **1987**, *38*, 163.
(2) Harris, A. L.; Brown, J. K.; Harris, C. B. *Annu. Rev. Phys. Chem.* **1988**, *39*, 341.
(3) Lienau, C.; Zewail, A. H. *J. Chim. Phys.* **1995**, *92*, 566.
(4) Hyde, M. G.; Beddard, G. S. *Chem. Phys.* **1991**, *151*, 239.
(5) Hyde, M. G.; Reid, G. D.; Beddard, G. S. *Chem. Phys. Lett.* **1992**, *190*, 130.

(6) Hirata, Y.; Ohta, M.; Okada, T.; Mataga, N. *J. Phys. Chem*. **1992**, *96*, 1517.
(7) Lenderink, E.; Duppen, K.; Wiersma, D. A. *Chem. Phys. Lett*. **1992**, *194*, 403.
(8) Meyer, A.; Nikowa, L.; Schroeder, J.; Schwarzer, D.; Thurau, G. *Faraday Discuss.* **1995**, *102*, 443.
(9) Scott, T. W.; Liu, S. N. *J. Phys. Chem.* **1989**, *93*, 1393.
(10) Hirata, Y., Niga; Y., Ohta, M.; Takizawa, M.; Okada, T. *Res. Chem. Intermed.* **1995**, *21*, 823.
(11) Ernsting, N. P. *Chem. Phys. Lett.* **1990**, *166*, 221.
(12) Hirata, Y.; Niga, Y.; Okada, T. *Chem. Phys. Lett.* **1994**, *221*, 283.
(13) Hirata, Y.; Niga, Y.; Makita, S.; Okada, T. *J. Phys. Chem. A* **1997**, *101*, 561.
(14) Bultmann, T.; Ernsting, N. P. *J. Phys. Chem.* **1996**, *100*, 19417.
(15) Rice, S. A. *Diffusion Controlled Reactions*; Bamford, C. H., Tipper, F. H., Compton, R. G., Eds.; Comprehensive Chemical Kinetics; Elsevier: Amsterdam, 1985; Vol. 25.
(16) Gupta, J. S.; Khakhar, D. V. *J. Chem. Phys*. **1997**, *107*, 1915.
(17) Shin, K. J.; Kapral, R. *J. Chem. Phys*. **1978**, *69*, 3685.
(18) Morine, G. H.; Kuntz, R. R. *Chem. Phys. Lett*. **1979**, *67*, 552.
(19) Otto, B.; Schroeder, J.; Troe, J. *J. Chem. Phys.* **1984**, *81*, 202.
(20) Ishizaka, S. *Appl. Phys. B* **1989**, *48*, 111.
(21) Bingemann, D.; Ernsting, N. P. *J. Chem. Phys.* **1995**, *102*, 2691.
(22) Kovalenko, S. A.; Ernsting, N. P.; Ruthmann, J. *Chem. Phys. Lett.* **1996**, *258*, 445.
(23) Smith, P. A. S.; Yu, T. Y. *J. Org. Chem.* **1987**, *17*, 1281.
(24) Moerke, W.; Jezierski, A.; Singer, H. *Z. F. Chem. Leipzig* **1979**, 147.
(25) Schmidt, U.; Mueller, A.; Markau, K. *Chem. Ber*. **1964**, *97*, 405.
(26) Feher, F.; Gladden, T.; Kurz, D. *Z. Naturforsch*. **1970**, *25B*, 1215.
(27) Maier, G. V.; Bazyl, O. K.; Artyukhov, V. Ya. *Opt. Spectrosc.* **1992**, *72*, 767.
(28) Lysak, N. A.; Mel'nichuk, S. V.; Tikhomirow, S. A.; Tolstorozhev, G. B. *J. Appl. Spectrosc.* **1988**, *49*, 1266.